Pedosphere **31**(1): 214–8, 2021
doi:10.1016/S1002-0160(20)60063-7
ISSN 1002-0160/CN 32-1315/P

Published by Elsevier B.V. and Science Press

PEDOSPHERE

www.elsevier.com/locate/pedosphere

Letter to the Editor

Global patterns of phosphorus transformation in relation to latitude, temperature and precipitation

Dear Editor,

Phosphorus (P) is essential and often a limiting nutrient for biological production on land and in the seas (Elser *et al*., 2007). The biologically available P to terrestrial and aquatic ecosystems ultimately derives from the continental weathering of rocks on the surface of the earth (Föllmi, 1996; Ruttenberg, 2003). Rocks are usually classified into three groups based on their origins: igneous, metamorphic, and sedimentary rocks. Although tectonic activity continually cycles the three rocks into each other, igneous rocks are the primary source rocks because they are formed *via* cooling and hardening of lava from the mantle and are a dominant rock pool, accounting for 65% of the mass, in the crust. Both sedimentary and metamorphic rocks are considered as secondary rocks. Sedimentary rocks are formed *via* accumulation of sediments derived from the weathering of pre-existing rocks and erosion of surface soils and often contain organic material of biological origin. Metamorphic rocks are formed *via* subduction of all rock types deep into the crust where they undergo metamorphisms under high pressure and temperature. Therefore, all the rocks currently present in the crust are believed to have first been igneous from the mantle. All the P that cycles through sedimentary rocks and biological systems must have been initially derived from continental weathering of crystalline rocks of igneous or metamorphic origin (Guidry *et al*., 2000; Horton, 2015).

The physicochemical characteristics of rock-forming mineral are often used to trace the origin of rock. The igneous and metamorphic rocks contain minerals that are formed under high temperature and pressure. In contrast, sedimentary rocks are formed in typical near-surface environments under low temperature and pressure. Many detritus minerals in sedimentary rocks are left over from pre-existing igneous and metamorphic rocks. Therefore, an understanding of the mineral composition of soil and sediment can provide the information needed to unlock the weathering processes in their source regions. The apatite family is the most abundant in the P-con- taining mineral among all rock types, with a general chemical composition as represented by the formula $Ca_{10}(PO_4)_6(OH,F,Cl)_2$. Different geological processes can induce variations in the OH, F, and Cl contents, resulting in different chemical stability within the apatite family members (Chang *et al*., 1998). In igneous rocks, F content increases as a result of fractional crystallization, and then fluorapatites become a dominant form (Nash, 1984). Apatites containing OH and Cl groups are more abundant in less-fractionated rock types. Sedimentary rocks are dominated by carbonate fluorapatites (CFAs) or francolites derived from the substitution of PO_4 with CO_3 (Nash, 1984; Chang *et al*., 1998).

Crystal structure and bonding energy control the chemical stability of the apatite family. In fluorapatite, two crystallographically different Ca atoms occupy different sites: one in seven-fold and the other in nine-fold coordination. Each F atom is surrounded by three Ca atoms, and Ca-O columns are linked with a hexagonal packed sphere of PO_4 group. The lengths of Ca-X (X = F, OH, or Cl) bond increase from F to OH and further to Cl (0.2311 nm for Ca-F in fluorapatite, 0.2385 nm for Ca-OH in hydroxyapatite, and 0.2759 nm for Ca-Cl in chlorapatite) (Hughes *et al.*, 1989). This bonding arrangement provides the most stable structure for fluorapatite. In contrast, the structures of hydroxyapatite and chlorapatite are stretched; thus, hydroxyapatites and chlorapatites are less stable. The chemical structures suggest that fluorapatites are the most resistant to weathering attack among the apatite family members. In contrast, bonding symmetry is distorted in CFAs as a result of carbonate substitution at phosphate site. This has been proved experimentally in kinetic studies on dissolution of igneous fluorapatites (IFAs) and sedimentary CFAs in aqueous solutions over a range of pH values (Guidry and MacKenzie, 2003; Chaïrat *et al*., 2007a, b).

Fluorapatites have been found to be the most common member of apatite family in the igneous rocks. As an early-formed, ubiquitous accessory mineral, IFAs are the principal repository of P in all igneous rocks. During weathering processes, IFAs are dissolved to release phosphate ions in aqueous solution, which are rapidly adsorbed to metal (Fe, Mn, Al, and Ca) oxides contained in soil and sediment or are assimilated into microbial and plant biomass. As soil ages, P might be transformed into CFAs and refractory organic P (Walker and Syers, 1976).

Based on the chronosequence of pedogenesis studies performed in New Zealand, Walker and Syers (1976) developed a conceptual model to simulate temporal changes

in soil P pools as a function of soil age. They postulated that at the beginning of soil development, all soil P is in primary mineral forms, mainly as calcium phosphate. As soil develops over time, the primary minerals weather rapidly and transform to occluded, non-occluded, and organic P, while total soil P declines due to leaching. Their model prediction suggested that at the late stage of soil development, soil P is low and is dominated by organic and occluded P. This conceptual model has been validated by numerous chronosequence studies in various ecosystems. Among these studies, the most convincing is the one demonstrating changes in soil P in the islands of Hawaii with soil age spanning thousands to millions of years as the volcanic islands were formed by the movement of the Pacific Plate over a stationary hotspot, a convective plume in the mantle, for millions of years, but under a similar subtropical oceanic climate (Crews *et al*., 1995; Vitousek *et al*., 1997; Chadwick *et al*., 1999). However, it should be noted that in all these chronosequence studies, the total apatite family was quantified as the so-called primary mineral P or apatite P since their sequential extraction methods used for fractionation of soil P pools did not distinguish between IFA and sedimentary CFA.

Sequential extraction has been an essential tool in all chronosequence studies to identify the forms of particulate P in soil and their evolution as a result of continental weathering and soil development on the surface of earth. It is a selective leaching procedure based on chemical reactivity of different solid P phases. The Hedley sequential extraction method has been widely used in the soil community (Hedley *et al*., 1982; Cross and Schlesinger, 1995; Tiessen and Moir, 2008; Yang and Post, 2011; Hou *et al*., 2016, 2018a). In this method, soil P sequential extraction consists of five steps. In the first step, anion resin is used to extract exchangeable inorganic phosphate, followed by treatment with $NaHCO_3$ solution (pH 8.5) to extract inorganic and organic P. In the third step, 0.1 mol L^{-1} NaOH solution is used for Fe and Al-bound P (occluded P), followed by treatment with 1 mol L^{-1} HCl solution for biogenic and detrital apatites. The final step is the digestion of residual solid sample in a strong acid with oxidants added to decompose refractory organic P. Many variations of this method currently used in soil analysis do not include a weak acid extraction step; thus, different forms of calcium phosphate, all together, are dissolved in a strong acid (*i.e.*, 1.0 mol L^{-1} HCl or 0.5 mol L^{-1} H_2SO_4). The caveat of these is, therefore, not making any distinction between biogenic/authigenic apatites and fluorapatites of igneous and metamorphic origins.

In order to quantify the authigenic CFA pool in marine sediments, Ruttenberg (1992) developed a sequential extraction method, the SEDEX method, in which a buffer solution of NH_4Ac (pH 4) extraction step is added to dissolve biogenic apatites before using 1 mol L^{-1} HCl to extract crystalline detrital apatites. The added step is Step 3 in the flow diagram in Fig. 1. The advantage of this method over the Hedley method is its ability to distinguish between CFA and detrital apatite of igneous or metamorphic origin (IFA). In the Hedley method, CFAs and IFAs are extracted together in a single strong acid step and are collectively called primary mineral P (Hou *et al*., 2018a). Although both CFAs and IFAs contain Ca and P as major elemental components, they have different biogeochemical origins and reactivities. Only the SEDEX method can separately quantify CFAs and IFAs in soil and sediment samples. Since IFAs are the primary P form in the igneous rocks at the beginning of weathering processes and their contents decrease progressively during the course of rock weathering and soil development, the absolute IFA content reflects the unweathered primary mineral P pool. All other forms of P are the products of transformation from original IFAs during weathering and soil development. The abundance of IFA relative to total P (TP) therefore reflects the status and extent (intensity and duration) of weathering in the study regions. In the subduction zone, IFAs remain in sediment, representing the pool of P escaping the biogeochemical cycle at the surface of earth, and eventually subduct into the mantle during rock tectonic cycles.

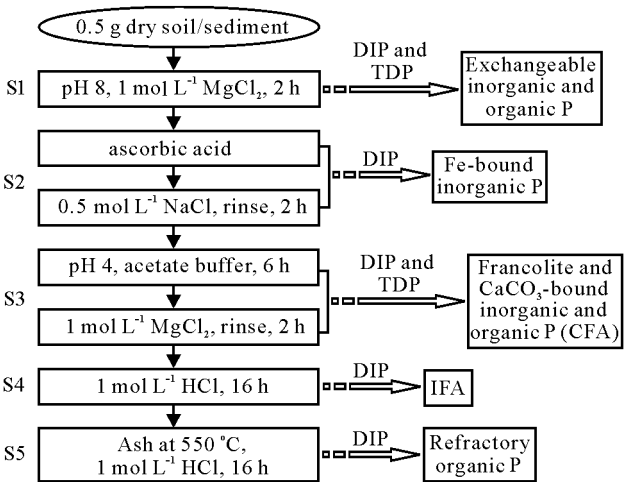

Fig. 1 Flow diagram of solid phase P fractionation (5 steps, S1–S5) using the SEDEX method (Ruttenberg, 1992; Zhang and Lanning, 2018) for soil and sediment samples: a solid sample (0.5 g, ground to < 125 μm) is sequentially extracted with 50 mL solutions of increasing reactivity at 25 °C, and at the end of the extraction step, particles are separated from solution. The vertical arrows indicate the sequence of extraction with the particulate residue from a previous step, and the horizontal arrows indicate the required P measurements in solution phase after separation by filtration. Dissolved organic P is calculated as the difference between total dissolved P (TDP) and dissolved inorganic P (DIP). CFA = carbonate fluorapatite; IFA = igneous fluorapatite.

Many previous studies have shown the effect of soil age on P transformation at ecosystem scales. These studies focused on the time dependence and kinetic nature of the weathering processes at local scales. Some recent studies have shown the effect of climate on P transformation at regional scales (Filippelli and Souch, 1999; Zhang *et al*., 2005; Feng *et al*., 2016; Siebers *et al*., 2017), and analyses

of global soil available P data using the Hedley method have demonstrated that soil available P is significantly affected by climate (Siebers *et al*., 2017; Hou *et al*., 2018b). Because of the inherent limitations of the Hedley method mentioned above, global patterns of P transformation in relation to climate forcing remain elusive. Here, we compiled an independent SEDEX dataset from the literature to identify the patterns of P transformation at the global scale in relation to climatic indices, such as absolute latitude (AL), mean annual temperature (MAT), and mean annual precipitation (MAP). This study will reveal how changes in TP, CFA, and IFA pools are related to climate conditions at the global scale.

The data used in this study were compiled from the published studies citing Ruttenberg (1992) through the Web of Science and Google Scholar search engines. To ensure data comparability, we used only data from the studies that reported solid phase P speciation analysis using the SEDEX method of Ruttenberg (1992) and the subsequent modifications (*e.g.*, Zhang *et al*., 2004, 2010; Zhang and Lanning, 2018). The advantage of these methods is the separation of IFAs from CFAs, as the former were the primary mineral and the latter are a weathering product. To discount the effect of anthropogenic influence on the natural P cycle, we limited our data to those studies which were located in the natural ecosystems on land and coastal waters in the continental shelf and did not include data from agricultural lands and aquatic systems that have been subjected to the impact of fertilizer application and wastewater discharge. To be representative of contemporary conditions on the surface of earth at a time scale of centuries, only samples taken from surface soil and sediment were used. In total, the database was drawn from 40 studies encompassing soils from North America (Levy and Schlesinger, 1999), Australia (Samadi and Gilkes, 1998), and Asia (Akhtar *et al*., 2014; Mehmood *et al*., 2018), deserts soils from Asia (Guo *et al*., 2011), Africa (Hudson-Edwards *et al*., 2014), and North America (Zhang *et al*., 2018), and sediments from rivers including the Amazon River (Berner and Rao, 1994), the Yangtze River (Rao and Berner, 1997; He *et al*., 2009; Hou *et al*., 2009; Ran *et al*., 2016), and the Yellow River (Yao *et al*., 2016), lakes (Njenga, 2005; Song *et al*., 2013), and estuarine and coastal waters (Ruttenberg and Berner, 1993; Vink *et al*., 1997; Eijsink *et al*., 2000; Schenau and De Lange, 2001; Liu *et al*., 2004, 2016; Zhang *et al*., 2004, 2010, 2016; Fang *et al*., 2007; Monbet *et al*., 2007; Virtasalo and Kotilainen, 2008; Yu *et al*., 2012; Berbel and Braga, 2014; Cong *et al*., 2014; Meng *et al*., 2014; Zhuang *et al*., 2014; Song and Liu, 2015; Yang *et al*., 2016, 2017, 2018; Kang *et al*., 2017; Sudheesh *et al*., 2017; Bastami *et al*., 2018). Surface sediment samples contain soil particles derived from the recent erosion of adjacent land surfaces; therefore, they contain the integrated weathering signals from the drainage basins of the studied rivers at a contemporary time scale. The sampling locations are shown in Fig. 2. The MAT and MAP data for each sampling site were extracted from original studies or, in absence of these data, from the WorldClim dataset (version 1.4). Pearson correlation analysis was carried out to quantify relationships between the contents of different P forms and AL, MAT, and MAP. As AL is linearly correlated with MAT, multiple linear regression was used to analyze correlations between the contents of different P forms and long-term MAT and MAP.

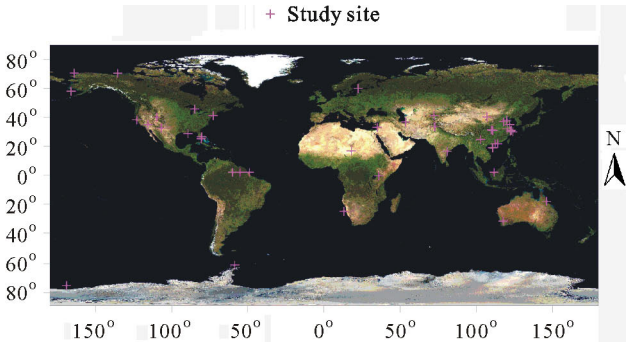

Fig. 2 Global distribution of samples used in the studies using the SEDEX method, a sequential extraction method developed by Ruttenberg (1992).

As shown in Fig. 1, the SEDEX dataset contains 40 studies distributed around the globe. These studies encompassed natural soils from deserts in Asia, Africa, and North America and sediments from lakes, rivers, and coastal waters. The river, lake, and coastal water sediments represent the integrated records of weathering in the drainage basins. In this dataset, the contents of TP in soil and sediment vary from 1.17 μmol g^{-1} in tropical Indonesia (Levy and Schlesinger, 1999) to 42.73 μmol g^{-1} on an Antarctic island (Berbel and Braga, 2014). In general, TP contents are low in the tropics and high in the high-latitude regions. The TP contents increase with AL, showing a significant positive correlation ($R^2 = 0.5377$, $P < 0.001$) (Table I, Fig. 3). In contrast, the TP contents decrease with local MAT, showing a significant negative correlation ($R^2 = 0.6031$, $P < 0.001$) (Table I, Fig. 3). This is consistent with results from previous regional studies in China, in which high TP contents were observed in cold, high-latitude regions, particularly in the frigid Taklamakan Desert, and low TP contents were observed in hot, tropical regions (Zhang *et al*., 2005; Feng *et al*., 2016).

The TP contents show a negative correlation with local MAP ($R^2 = 0.1848$, $P < 0.001$), indicating that high TP occurs in arid climate regions and low TP is associated with wet, tropical climate. The decreasing trends in TP with MAT and MAP are in agreement with an independent dataset generated using the Hedley method (Hou *et al*., 2018b). The global pattern of TP reveals the climate to be a dominant driving force in continental rock weathering and terrestrial P cycling. It is well known that high temperature and precipitation enhance rock weathering (Maher and Chamberlain,

TABLE I

Multiple regression equations obtained and associated R^2 and P values describing the explanatory capability of each model for the relationships of different P forms with absolute latitude (AL, *) and mean annual temperature (MAT, °C) and precipitation (MAP, mm year^{-1}) of the study sites

P form (y)[a)]	Equation	R^2	P value
TP	$y = 3.231384 + 0.414703$AL	0.5377	< 0.001
	$y = 27.72849 - 0.72982$MAT	0.6031	< 0.001
	$y = 22.74002 - 0.00689$MAP	0.1848	< 0.001
	$y = 27.15295 - 0.77739$MAT $+ 0.001311$MAP	0.6073	< 0.001
Exch-P	$y = 0.446073 + 0.012779$AL	0.1252	< 0.001
	$y = 1.13555 - 0.01858$MAT	0.0958	< 0.001
	$y = 0.877341 - 0.00005$MAP	0.0024	0.452
	$y = 1.031572 - 0.02717$MAT $+ 0.00237$MAP	0.1289	< 0.001
Fe-P	$y = -0.40926 + 0.074153$AL	0.3503	< 0.001
	$y = 3.748385 - 0.11717$MAT	0.3167	< 0.001
	$y = 3.37243 - 0.00151$MAP	0.1816	< 0.001
	$y = 3.9452 - 0.1009$MAT $- 0.00045$MAP	0.3266	< 0.001
CFA	$y = 0.701953 + 0.126958$AL	0.3438	< 0.001
	$y = 8.135391 - 0.21947$MAT	0.3720	< 0.001
	$y = 7.379517 - 0.00278$MAP	0.2059	< 0.001
	$y = 8.468898 - 0.19191$MAT $- 0.00076$MAP	0.3815	< 0.001
IFA	$y = 0.252176 + 0.188518$AL	0.4053	< 0.001
	$y = 11.76748 - 0.35448$MAT	0.5190	< 0.001
	$y = 9.077126 - 0.00309$MAP	0.1357	< 0.001
	$y = 11.30591 - 0.39263$MAT $+ 0.001051$MAP	0.5287	< 0.001
Ref-OP	$y = 2.356125 + 0.005479$AL	0.0023	0.454
	$y = 2.635391 - 0.00698$MAT	0.0014	0.565
	$y = 1.833148 + 0.000656$MAP	0.0421	0.001
	$y = 2.116317 - 0.04988$MAT $+ 0.001182$MAP	0.0857	< 0.001

[a)] TP = total P; Exch-P = exchangeable P; Fe-P = Fe-bound P; CFA = carbonate fluorapatites or francolite; IFA = igneous fluorapatite; Ref-OP = refractory organic P.

2014), supplying essential nutrient P to support high biological productivity. Enhanced chemical weathering and hydrological transport as well as biological uptake result in low TP in soil and sediment. Climate-driven soil erosion, particularly the loss of fine-grained particles, and leaching of dissolved phosphate and dissolved organic P are major sinks for terrestrial P reservoirs (Chadwick *et al*., 2003; Mishra *et al*., 2013). As a result, high runoff induced by heavy precipitation that breaks the transport limitation can significantly reduce TP content in regions with tropical and subtropical climate (Maher and Chamberlain, 2014).

The contents of IFAs in soil and sediment vary from 0.17 μmol g^{-1} in tropical Indonesia (Levy and Schlesinger, 1999) to 23.72 μmol g^{-1} on an Antarctic island (Berbel and Braga, 2014). Similar to TP, IFAs are low in the tropics and high in the high-latitude regions. The IFA contents also increase with AL, showing a positive correlation ($R^2 = 0.4053$ and $P < 0.001$) (Table I, Fig. 3). The abundance of IFAs relative to TP increases from 24% in the tropics to 44% in the high-latitude regions. In contrast, IFA contents decrease with MAT, showing a significant negative correlation ($R^2 = 0.5190$, $P < 0.001$) (Table I, Fig. 3). This is in agreement with the observed high IFA contents in cold, high-latitude regions and low IFA contents in warm, subtropical regions, *e.g.*, about 0.3 μmol g^{-1} in Florida Bay, USA (Zhang *et al*., 2004). The IFA contents also show a negative correlation with MAP ($R^2 = 0.1357$, $P < 0.001$), indicating that the high IFA contents are associated with arid climate such as the Loess Plateau of northern China and low IFAs are associated with wet, tropical climate. The global pattern of IFAs reveals the climate as a dominant driving force in continental weathering of IFAs. It is well known that high temperature enhances weathering and dissolution of IFA to dissolved phosphate (Guidry and MacKenzie, 2003), which is immediately assimilated by plants and soil microbes. Enhanced weathering and biological uptake result in low IFA content in soil and sediment. Since IFAs typically occur in fine particles, soil erosion induced by heavy precipitation can significantly drain IFAs from terrestrial surface.

The CFAs are carbonate-associated apatites of biological origin and most commonly occur in sedimentary phosphorites. In this dataset, the CFA contents vary from 0.23 to 18.77 μmol g^{-1}, typically accounting for about 30% of TP. Similar to TP and IFAs, CFAs significantly increase with AL and decreases with MAT and MAP ($R^2 = 0.3438$, 0.3720, and 0.2059, respectively, $P < 0.001$) (Table I, Fig. 3). The Fe-P contents vary from 0.05 to 11.5 μmol g^{-1}, typically accounting for about 20% of TP. Similar to TP, Fe-P significantly increased with AL and decreased with MAT and MAP ($R^2 = 0.3503$, 0.3167, and 0.1816, respectively, $P < 0.001$) (Table I, Fig. 3). The high degree of scatter reflects the ubiquitous, variable abundance of iron associated with variation in bedrock lithology in terrestrial surface environments. The Fe-P increase with AL is because TP increases with AL. It seems that TP (or exchangeable P (Exch-P)) controls Fe-P and available Fe does not regulate the amount of Fe-P. This has been demonstrated in regional studies, for example, in Florida Bay, USA (Zhang *et al*., 2004; Zhang and Huang, 2007).

The Ref-OP contents range from 0.22 to 10.1 μmol g^{-1}, typically accounting for about 20% of TP, vary little with AL or MAT ($P > 0.05$), but increase with MAP ($P = 0.001$), all showing significant scatter ($R^2 = 0.0024$, 0.0014, and 0.0421, respectively) (Table I, Fig. 3). The higher Ref-OP contents in the temperate regions reflect higher biomass in this region, as this P pool is derived from and accumulated as a result of biological activity. In arid and semiarid environments, water availability can limit plant biomass, resulting in a small pool of Ref-OP (Brantley *et al*., 2011; Margalef *et al*., 2017). The increasing trend of Ref-OP with MAP is in agreement with those of observations.

The Exch-P fraction represents the immediately bioavailable P pool in soil and sediment. This fraction varies from 0.01 to 2.52 μmol g^{-1}, typically accounting for less than 10% of TP. Similar to TP, the Exch-P contents increase

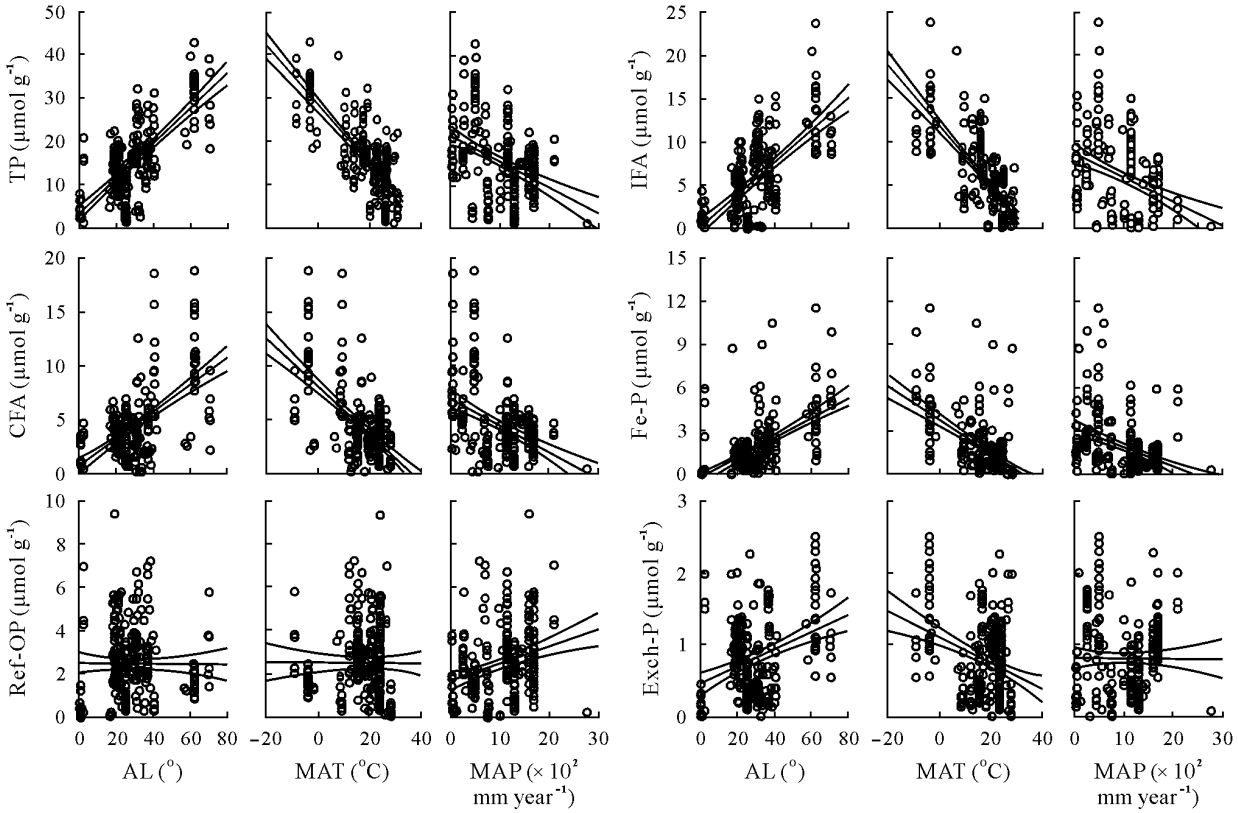

Fig. 3 Relationships of total P (TP), igneous fluorapatite (IFA), carbonate fluorapatite (CFA) or francolite, Fe-bound P (Fe-P), refractory organic P (Ref-OP), and exchangeable P (Exch-P) contents with absolute latitude (AL), mean annual temperature (MAT), and mean annual precipitation (MAP), fitted by linear regression with 95% confidence intervals.

with AL and decrease with MAT with significant scatter ($R^2 = 0.1252$ and 0.0958, respectively) (Table I, Fig. 3). The latitude and temperature trends of Exch-P are consistent with those of TP because the nearly constant proportions of Exch-P in TP have been observed worldwide. However, the significant scatter reflects that the other variables such as chemical composition and particle size of soil and sediment might also play roles other than TP. In contrast, Exch-P shows no significant correlation with MAP (a negligible slope of -0.00005, $R^2 = 0.0024$, $P = 0.452$) (Table I, Fig. 3).

With limited available SEDEX data, we have provided a broad-brush picture of global patterns of the terrestrial P biogeochemical cycle. A linear pattern has been observed between the P pool and AL, MAT, and MAP. Averaged latitudinal gradients for different forms of P are shown in Fig. 4. The pools of TP, IFAs, CFAs, and Fe-P all increase with increasing AL. The TP contents increase from about 4 μmol g^{-1} in the tropics to about 36 μmol g^{-1} in the polar regions. The IFA pool is dominant from the subtropics to high-latitude regions, accounting for below 30% of TP in the subtropics and 42% in the high-latitude regions. The CFA pool is the second largest, ranging from 2 μmol g^{-1} in the tropics to 10 μmol g^{-1} in the polar regions. The ratios of CFAs to TP vary little with AL from 23% in the tropics to 30% in the high-latitude regions. The Fe-P pool accounts for less than 5% of TP in the tropics and about

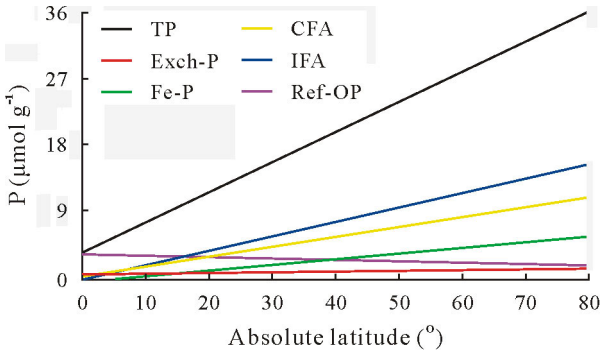

Fig. 4 Average latitudinal gradients of total P (TP) and five different forms of P separated using the SEDEX method (Ruttenberg, 1992). TP = total P; IFA = igneous fluorapatite; CFA = carbonate fluorapatite or francolite; Fe-P = Fe-bound P; Ref-OP = refractory organic P; Exch-P = exchangeable P.

15% of TP in the high-latitude regions. The Exch-P pool is the smallest, but represents the most bioavailable form of P in the surface environment, varying from 0.5 to 1.5 μmol g^{-1} and accounting for 10% of TP in the tropics and 4% of TP in the high-latitude regions due to relatively high TP in the cold regions. The Ref-OP pool is the sole fraction that shows no clear trend with AL. It has a global average content of 2.6 μmol g^{-1} and accounts for about 10% of TP in the temperate and high-latitude regions, but become a significant P form (30% of TP) in the tropics, where TP is typically

low. The global patterns shown in Fig. 4 are a result of the combined actions of physical erosion, chemical weathering, hydrological transport, biological uptake, and recycling of various P forms in the earth surface environment. We believe that the driving force behind all these actions is climate, which in turn is governed by a latitudinal gradient in the distribution of solar irradiance energy around the globe.

ACKNOWLEDGEMENT

This study was supported by the National Oceanic and Atmospheric Administration (NOAA) Ocean and Atmospheric Research, USA. The scientific results and conclusions, and any views or opinions expressed herein are those of the author and do not necessarily reflect the views of NOAA or Department of Commerce, USA.

REFERENCES

Akhtar M S, Imran M, Mehmood A, Memon M, Rukh S, Kiani G S. 2014. Apatite loss in Pothwar Loess Plain (Pakistan) fits a simple linear reservoir model. *Pedosphere*. **24**: 763–775.

Bastami K D, Neyestani M R, Raeisi H, Shafeian E, Baniamam M, Shirzadi A, Esmaeilzadeh M, Mozaffari S, Shahrokhi B. 2018. Bioavailability and geochemical speciation of phosphorus in surface sediments of the southern Caspian Sea. *Mar Pollut Bull*. **126**: 51–57.

Berbel G B B, Braga E S. 2014. Phosphorus in Antarctic surface marine sediments—chemical speciation in Admiralty bay. *Antarct Sci*. **26**: 281–289.

Berner R A, Rao J L. 1994. Phosphorus in sediments of the Amazon River and estuary: Implications for the global flux of phosphorus to the sea. *Geochim Cosmochim Acta*. **58**: 2333–2339.

Brantley S L, Megonigal J P, Scatena F N, Balogh-Brunstad Z, Barnes R T, Bruns M A, van Cappellen P, Dontsova K, Hartnett H E, Hartshorn A S, Heimsath A, Herndon E, Jin L, Keller C K, Leake J R, McDowell W H, Meinzer F C, Mozdzer T J, Petsch S, Pett-Ridge J, Pregitzer K S, Raymond P A, Riebe C S, Shumaker K, Sutton-Grier A, Walter R, Yoo K. 2011. Twelve testable hypotheses on the geobiology of weathering. *Geobiology*. **9**: 140–165.

Chadwick O A, Derry L A, Vitousek P M, Huebert B J, Hedin L O. 1999. Changing sources of nutrients during four million years of ecosystem development. *Nature*. **397**: 491–497.

Chadwick O A, Gavenda R T, Kelly E F, Ziegler K, Olson C G, Elliott W C, Hendricks D M. 2003. The impact of climate on the biogeochemical functioning of volcanic soils. *Chem Geol*. **202**: 195–223.

Chaïrat C, Oelkers E H, Schott J, Lartigue J E. 2007a. Fluorapatite surface composition in aqueous solution deduced from potentiometric, electrokinetic, and solubility measurements, and spectroscopic observations. *Geochim Cosmochim Acta*. **71**: 5888–5900.

Chaïrat C, Schott J, Oelkers E H, Lartigue J E, Harouiya N. 2007b. Kinetics and mechanism of natural fluorapatite dissolution at 25°C and pH from 3 to 12. *Geochim Cosmochim Acta*. **71**: 5901–5912.

Chang L L Y, Howie R A, Zussman J. 1998. Rock forming minerals. *In* Chang L L Y, Howie R A, Zussman J (eds.) Non-silicates: Sulphates, Carbonates, Phosphates, Halides. 2nd Edn. The Geological Society, London. pp. 297–334**.**

Cong M, Jiang T, Qi Y Z, Dong H P, Teng D Q, Lu S H. 2014. Phosphorus forms and distribution in Zhejiang coastal sediment in the East China Sea. *Int J Sediment Res*. **29**: 278–284.

Crews T E, Kitayama K, Fownes J H, Riley R H, Herbert D A, Mueller-Dombois D, Vitousek P M. 1995. Changes in soil phosphorus fractions and ecosystem dynamics across a long chronosequence in Hawaii. *Ecology*. **76**: 1407–1424.

Cross A F, Schlesinger W H. 1995. A literature review and evaluation of the Hedley fractionation: Applications to the biogeochemical cycle of soil phosphorus in natural ecosystems. *Geoderma*. **64**: 197–214.

Eijsink L M, Krom M D, Herut B. 2000. Speciation and burial flux of phosphorus in the surface sediments of the eastern Mediterranean. *Am J Sci*. **300**: 483–503.

Elser J J, Bracken M E S, Cleland E E, Gruner D S, Harpole W S, Hillebrand H, Ngai J T, Seabloom E W, Shurin J B, Smith J E. 2007. Global analysis of nitrogen and phosphorus limitation of primary producers in freshwater, marine and terrestrial ecosystems. *Ecol Lett*. **10**: 1135–1142.

Fang T H, Chen J L, Huh C A. 2007. Sedimentary phosphorus species and sedimentation flux in the East China Sea. *Cont Shelf Res*. **27**: 1465–1476.

Feng J, Turner B L, Lü X T, Chen Z H, Wei K, Tian J H, Wang C, Luo W T, Chen L J. 2016. Phosphorus transformations along a large-scale climosequence in arid and semiarid grasslands of northern China. *Glob Biogeochem Cycl*. **30**: 1264–1275.

Filippelli G M, Souch C. 1999. Effects of climate and landscape development on the terrestrial phosphorus cycle. *Geology*. **27**: 171–174.

Föllmi K B. 1996. The phosphorus cycle, phosphogenesis and marine phosphate-rich deposits. *Earth-Sci Rev*. **40**: 55–124.

Guidry M W, Mackenzie F T, Arvidson R S. 2000. Role of tectonics in phosphorus distribution and cycling. *In* Glenn C R, Prévôt-Lucas L, Lucas J (eds.) Marine Authigenesis: From Global to Microbial. Society for Sedimentary Geology, Tulsa. pp. 35–51.

Guidry M W, MacKenzie F T. 2003. Experimental study of igneous and sedimentary apatite dissolution: Control of pH, distance from equilibrium, and temperature on dissolution rates. *Geochim Cosmochim Acta*. **67**: 2949–2963.

Guo B S, Yang H W, Li Y. 2011. The speciation of phosphorus in the sand particles in western Inner Mongolia. *In* Institute of Electrical and Electronics Engineers (IEEE) (ed.) Proceedings of the 2011 2nd International Conference on Mechanic Automation and Control Engineering. IEEE, Hohhot. pp. 2755–2757.

He H J, Chen H T, Yao Q Z, Qin Y W, Mi T Z, Yu Z G. 2009. Behavior of different phosphorus species in suspended particulate matter in the Changjiang estuary. *Chin J Oceanogr Limnol*. **27**: 859–868.

Hedley M J, Stewart J W B, Chauhan B S. 1982. Changes in inorganic and organic soil phosphorus fractions induced by cultivation practices and by laboratory incubations. *Soil Sci Soc Am J*. **46**: 970–976.

Horton F. 2015. Did phosphorus derived from the weathering of large igneous provinces fertilize the Neoproterozoic ocean? *Geochem Geophys Geosyst*. **16**: 1723–1738.

Hou E Q, Chen C R, Kuang Y W, Zhang Y G, Heenan M, Wen D Z. 2016. A structural equation model analysis of phosphorus transformations in global unfertilized and uncultivated soils. *Glob Biogeochem Cycl*. **30**: 1300–1309.

Hou E Q, Tan X, Heenan M, Wen D Z. 2018a. A global dataset of plant available and unavailable phosphorus in natural soils derived by Hedley method. *Sci Data.* **5**: 180166.

Hou E Q, Chen C R, Luo Y Q, Zhou G Y, Kuang Y W, Zhang Y G, Heenan M, Lu X K, Wen D Z. 2018b. Effects of climate on soil phosphorus cycle and availability in natural terrestrial ecosystems. *Glob Change Biol*. **24**: 3344–3356.

Hou L J, Liu M, Yang Y, Ou D N, Lin X, Chen H, Xu S Y. 2009. Phosphorus speciation and availability in intertidal sediments of the Yangtze estuary, China. *Appl Geochem*. **24**: 120–128.

Hudson-Edwards K A, Bristow C S, Cibin G, Mason G, Peacock C L. 2014. Solid-phase phosphorus speciation in Saharan Bodélé depression dusts and source sediments. *Chem Geol*. **384**: 16–26.

Hughes J M, Cameron M, Crowley K D. 1989. Structural variations in natural F, OH, and Cl apatites. *Am Mineral*. **74**: 870–876.

Kang X M, Song J M, Yuan H M, Shi X, Yang W F, Li X G, Li N, Duan L Q. 2017. Phosphorus speciation and its bioavailability in sediments of the Jiaozhou Bay. *Estuar Coast Shelf Sci*. **188**: 127–136.

Levy E T, Schlesinger W H. 1999. A comparison of fractionation methods for forms of phosphorus in soils. *Biogeochemistry*. **47**: 25–38.

Liu J, Zang J Y, Zhao C Y, Yu Z G, Xu B C, Li J X, Ran X B. 2016. Phosphorus speciation, transformation, and preservation in the coastal area of Rushan Bay. *Sci Total Environ*. **565**: 258–270.

Liu S M, Zhang J, Li D J. 2004. Phosphorus cycling in sediments of the Bohai and Yellow Seas. *Estuar Coast Shelf Sci*. **59**: 209–218.

Maher K, Chamberlain C P. 2014. Hydrologic regulation of chemical weathering and the geologic carbon cycle. *Science*. **343**: 1502–1504.

Margalef O, Sardans J, Fernández-Martínez M, Molowny-Horas R, Janssens I A, Ciais P, Richter D G A, Obersteiner M, Asensio D, Peñuelas J. 2017. Global patterns of phosphatase activity in natural soils. *Sci Rep*. **7**: 1337.

Mehmood A, Akhtar M S, Imran M, Rukh S. 2018. Soil apatite loss rate across different parent materials. *Geoderma*. **310**: 218–229.

Meng J, Yao P, Yu Z G, Bianchi T S, Zhao B, Pan H H, Li D. 2014. Speciation, bioavailability and preservation of phosphorus in surface sediments of the Changjiang estuary and adjacent East China Sea inner shelf. *Estuar Coast Shelf Sci*. **144**: 27–38.

Mishra A, Tripathi J K, Mehta P, Rajamani V. 2013. Phosphorus distribution and fractionation during weathering of amphibolites and gneisses in different climatic setups of the Kaveri River catchment, India. *Appl Geochem*. **33**: 173–181.

Monbet P, Brunskill G J, Zagorskis I, Pfitzner J. 2007. Phosphorus speciation in the sediment and mass balance for the central region of the Great Barrier Reef continental shelf (Australia). *Geochim Cosmochim Acta*. **71**: 2762–2779.

Nash W P. 1984. Phosphate minerals in terrestrial igneous and metamorphic rocks. *In*. Nriagu J O, Moore P B (eds.) Phosphate Minerals. Springer, Berlin, Heidelberg. pp. 215–241.

Njenga J. 2005. The geochemistry of the sediments of three tropical lakes: Nakuru, Naivasha (Kenya) and Kolleru (India). Ph.D. thesis, Jawaharlal Nehru University.

Ran X B, Chen H T, Wei J F, Yao Q Z, Mi T Z, Yu Z G. 2016. Phosphorus speciation, transformation and retention in the Three Gorges Reservoir, China. *Mar Freshw Res*. **67**: 173–186.

Rao J L, Berner R A. 1997. Time variations of phosphorus and sources of sediments beneath the Chang Jiang (Yangtze River). *Mar Geol*. **139**: 95–108.

Ruttenberg K C. 1992. Development of a sequential extraction method for different forms of phosphorus in marine sediments. *Limnol Oceanogr*. **37**: 1460–1482.

Ruttenberg K C, Berner R A. 1993. Authigenic apatite formation and burial in sediments from non-upwelling, continental margin environments. *Geochim Cosmoch Acta*. **57**: 991–1007.

Ruttenberg K C. 2003. The global phosphorus cycle. *Treatise Geochem*. **8**: 585–643.

Samadi A, Gilkes R J. 1998. Forms of phosphorus in virgin and fertilised calcareous soils of Western Australia. *Aust J Soil Res*. **36**: 585–602.

Schenau S J, De Lange G J. 2001. Phosphorus regeneration *vs.* burial in sediments of the Arabian Sea. *Mar Chem*. **75**: 201–217.

Siebers N, Sumann M, Kaiser K, Amelung W. 2017. Climatic effects on phosphorus fractions of native and cultivated North American grassland soils. *Soil Sci Soc Am J*. **81**: 299–309.

Song G D, Liu S M. 2015. Phosphorus speciation and distribution in surface sediments of the Yellow Sea and East China Sea and potential impacts on ecosystem. *Acta Oceanol Sin*. **34**: 84–91.

Song Y Y, Feng M H, Su Z G, Pan J Z, Li W C. 2013. Vertical distribution of chemical speciation of phosphorus in sediments from different sources of Fuxian Lake. *Acta Sci Circumst* (in Chinese). **33**: 2579–2589.

Sudheesh V, Movitha M, Hatha A A M, Renjith K R, Resmi P, Rahiman M, Nair S M. 2017. Effects of seasonal anoxia on the distribution of phosphorus fractions in the surface sediments of southeastern Arabian Sea shelf. *Cont Shelf Res*. **150**: 57–64.

Tiessen H, Moir J O. 2008. Characterization of available P by sequential extraction. *In* Carter M R, Gregorich E G (eds.) Soil Sampling and Methods of Analysis. 2nd Edn. CRC Press, Boca Raton. pp. 293–306.

Vink S, Chambers R M, Smith S V. 1997. Distribution of phosphorus in sediments from Tomales Bay, California. *Mar Geol*. **139**: 157–179.

Virtasalo J J, Kotilainen A T. 2008. Phosphorus forms and reactive iron in lateglacial, postglacial and brackish-water sediments of the Archipelago Sea, northern Baltic Sea. *Mar Geol*. **252**: 1–12.

Vitousek P M, Chadwick O A, Crews T E, Fownes J H, Hendricks D M, Herbert D. 1997. Soil and ecosystem development across the Hawaiian Islands. *GSA Today*. **7**: 1–8.

Walker T W, Syers J K. 1976. The fate of phosphorus during pedogenesis. *Geoderma*. **15**: 1–19.

Yang B, Liu S M, Wu Y, Zhang J. 2016. Phosphorus speciation and availability in sediments off the eastern coast of Hainan Island, South China Sea. *Cont Shelf Res*. **118**: 111–127.

Yang B, Song G D, Liu S M, Jin J. 2017. Phosphorus recycling and burial in core sediments of the East China Sea. *Mar Chem*. **192**: 59–72.

Yang B, Liu S M, Zhang G L. 2018. Geochemical characteristics of phosphorus in surface sediments from the continental shelf region of the northern South China Sea. *Mar Chem*. **198**: 44–55.

Yang X, Post W M. 2011. Phosphorus transformations as a function of pedogenesis: A synthesis of soil phosphorus data using Hedley fractionation method. *Biogeosciences*. **8**: 2907–2916.

Yao Q Z, Du J T, Chen H T, Yu Z G. 2016. Particle-size distribution and phosphorus forms as a function of hydrological forcing in the Yellow River. *Environ Sci Pollut Res*. **23**: 3385–3398.

Yu Y, Song J M, Li X G, Duan L Q. 2012. Geochemical records of decadal variations in terrestrial input and recent anthropogenic eutrophication in the Changjiang estuary and its adjacent waters. *Appl Geochem*. **27**: 1556–1566.

Zhang C, Tian H Q, Liu J Y, Wang S Q, Liu M L, Pan S F, Shi X Z. 2005. Pools and distributions of soil phosphorus in China. *Glob Biogeochem Cycl*. **19**: GB1020.

Zhang J Z, Fischer C J, Ortner P B. 2004. Potential availability of sedimentary phosphorus to sediment resuspension in Florida Bay. *Glob Biogeochem Cycl*. **18**: GB4008.

Zhang J Z, Huang X L. 2007. Relative importance of solid-phase phosphorus and iron on the sorption behavior of sediments. *Environ Sci Technol*. **41**: 2789–2795.

Zhang J Z, Guo L D, Fischer C J. 2010. Abundance and chemical speciation of phosphorus in sediments of the Mackenzie River Delta, the Chukchi Sea and the Bering Sea: Importance of detrital apatite. *Aquat Geochem*. **16**: 353–371.

Zhang J Z, Lanning N T. 2018. Ascorbic acid as a reductant for extraction of iron-bound phosphorus in soil samples: A method comparison study. *Commun Soil Sci Plant Anal.* **49**: 2155–2161.

Zhang Y, Gao X L, Wang C Y, Chen C T A, Zhou F X, Yang Y W. 2016. Geochemistry of phosphorus in sediment cores from Sishili Bay, China. *Mar Pollut Bull*. **113**: 552–558.

Zhang Z J, Goldstein H L, Reynolds R L, Hu Y F, Wang X M, Zhu M Q. 2018. Phosphorus speciation and solubility in aeolian dust deposited in the interior American West. *Environ Sci Technol*. **52**: 2658–2667.

Zhuang W, Gao X L, Zhang Y, Xing Q G, Tosi L, Qin S. 2014. Geochemical characteristics of phosphorus in surface sediments of two major Chinese mariculture areas: The Laizhou Bay and the coastal waters of the Zhangzi Island. *Mar Pollut Bull*. **83**: 343–351.

Jia-Zhong ZHANG*

Ocean Chemistry and Ecosystems Division, Atlantic Oceanographic and Meteorological Laboratory, National Oceanic and Atmospheric Administration, Miami FL 33149 (USA)

(Received August 22, 2019; revised October 8, 2019)

*Corresponding author. E-mail: Jia-Zhong.Zhang@noaa.gov.